J Appl Electrochem (2008) 38:437–444
DOI 10.1007/s10800-007-9456-4

ORIGINAL PAPER

Influence of alloying and microstructure on the electrochemical hydriding of TiNi-based ternary alloys

Boris Drenchev · Tony Spassov · Dimitar Radev

Received: 11 July 2007 / Revised: 19 November 2007 / Accepted: 21 November 2007 / Published online: 7 December 2007

Abstract Nanostructured ternary TiNi-type alloys, namely $Ti_{0.8}M_{0.2}Ni$ (M = Zr, V), $TiNi_{0.8}N_{0.2}$ (N = Cu, Mn) and $TiNi_{1-x}Mn_x$ (x = 0.2, 0.4, 0.6, 1.0), were synthesized by mechanical alloying. Depending on the intensity and time of milling alloys with different microstructure were obtained. The as-milled $TiNi_{1-x}Mn_x$ alloys contain substantial amount of amorphous phase, which crystallizes during annealing. Annealing of the as-milled fine nanocrystalline materials at 500 °C results only in slight coarsening of the microstructure, which remains still nanocrystalline. Fully crystalline material (with crystal size larger than 50 nm), consisting of mainly cubic TiNi was obtained by annealing the ball-milled alloys at $T \geq 700$ °C. Electrochemical hydrogen charge/discharge cycling of the as-milled as well as of annealed alloys were carried out at galvanostatic conditions. It was found that among the nanocrystalline $Ti_{0.8}M_{0.2}Ni_{0.8}N_{0.2}$ (M = Zr, V; N = Cu, Mn) alloys $TiNi_{0.8}Mn_{0.2}$ revealed the highest discharge capacity of 56 mAh g^{-1} in the as-milled state and 75 mAh g^{-1} after short-time annealing at 500 °C. Annealing at higher temperature does not increase the capacity further. The as-milled $TiNi_{1-x}Mn_x$ alloys with $x \leq 0.4$ reveal noticeably higher discharge capacity and better cycle life than the Mn-richer alloys. Based on potentiostatic experiments the diffusion coefficients of hydrogen into TiNi alloys in two different microstructural states (fine and coarser nanocrystalline) as well as in as-milled amorphous/nanocrystalline and nanocrystalline $TiNi_{0.8}Mn_{0.2}$ were determined. The hydrogen diffusion coefficients of the TiNi alloys are comparable (1.9–2.7 × 10^{-12} cm^2 s^{-1}). The diffusion coefficient in the as-milled amorphous/nanocrystalline $TiNi_{0.8}Mn_{0.2}$ was found to be 3–4 times higher than that of the as-milled nanocrystalline alloy.

Keywords Ti–Ni alloys · Nanostructured alloys · Electrochemical hydriding · Discharge capacity · Hydrogen diffusivity

1 Introduction

The application of titanium alloys as electrode materials for Ni-MH batteries has recently attracted substantial interest [1–17]. Various alloying elements have been used to improve the electrochemical capacity and cycle life of TiNi-and TiFe-based ternary and quaternary alloys. Ni replacement by Mg, Mn or Zr improves the discharge capacity and cycle life of the electrodes prepared from TiNi alloys [12]. Substituting Nb and Pd for Ni enhances markedly the cycle life of TiNi electrodes as well [13]. A capacity of 155 mAh g^{-1} and relatively fast activation was achieved for $TiNi_{0.75}Fe_{0.25}$ [6]. Similar electrode characteristics were obtained for TiNi with partial Ni replacement by Mg or Mn [12]. Mn or Ni substitution for Fe in TiFe-based AB alloys showed good gravimetric and volumetric reversible hydrogen capacity [15]. However, $TiFe_{0.8}Ni_{0.2}$ revealed low capacity and low plateau pressure [15]. Partial substitution of Co or Ni for Fe in FeTi was found to result in solid solution formation and the detected decrease of the plateau pressure was ascribed to the different hydride formation enthalpies of TiFe, TiNi and TiCo [16].

B. Drenchev · T. Spassov (✉)
Department of Chemistry, University of Sofia "St.Kl.Ohridski", 1164 Sofia, Bulgaria
e-mail: tspassov@chem.uni-sofia.bg

D. Radev
Institute of General and Inorganic Chemistry, BAS, 1113 Sofia, Bulgaria

Hydrogen solubility and diffusivity in cubic NiTi were obtained in the temperature range of 500–950 °C and hydrogen gas pressure of up to 1.3 bar [17]. The enthalpy of hydrogen solution per H atom was determined to be 183 ± 40 meV and the activation energy of hydrogen diffusion -480 ± 50 meV [17].

Nanocrystalline Ti-based alloys show substantially enhanced hydrogen sorption properties compared to the conventional polycrystalline materials [6, 8, 10, 12]. Amorphous TiNi alloys were found to be very easily activated as well [8]. Ball milling is the most frequently applied method for producing nanostructured and amorphous Ti based materials for hydrogen storage [6, 9, 10, 12, 14]. The reduction of the powder particles size and creation of new surfaces during ball milling results in considerable improvement of the initial rate of hydrogen absorption/desorption and consequently to reduced activation periods. Ball milling with subsequent annealing could also result in a nanostructured materials with appropriate for hydrogen storage characteristics [6, 9, 14].

Our recent work [14] was focused on the electrochemical hydriding/dehydridng of amorphous and nanocrystalline $TiNi_{1-x}M_x$ (M = Co, Fe, Sn; $x = 0$ and 0.2) alloys, synthesized by mechanical alloying. It was found that among the studied alloys $TiNi_{0.8}Fe_{0.2}$ revealed the highest discharge capacity of about 65 mAh g^{-1} in the as-milled state and 80 mAh g^{-1} after annealing at 500 °C. As a continuation of this study the present work aims at investigating the influence of different alloying elements (Zr, V, Cu, Mn), replacing both Ti and Ni, and the microstructure on the electrochemical hydriding of ternary TiNi-type alloys.

2 Experimental part

Powders of Ni (99.5%), Ti (99.7%), Zr (>99%), Cu (>99%), V (>99%) and Mn (99.8%) in appropriate amounts were mixed together in the reactors of a self-constructed high-energy planetary mill to produce TiNi, $TiNi_{0.8}Cu_{0.2}$, $TiNi_{0.8}Mn_{0.2}$ and $Ti_{0.8}Zr_{0.2}Ni$, $Ti_{0.8}V_{0.2}Ni$. A previous study of ours [14] indicated that the alloying started after about 5 h of milling at ball to powder mass ratio of 9:1 under argon atmosphere (n-heptane) and ended after 10.5 h. After each 1 h of continuous milling 30 min relaxation time was applied. For the second series of alloys ($TiNi_{1-x}Mn_x$; $x = 0.2$, 0.4, 0.6, 1.0) the reagents were mixed and mechanically activated in a planetary mill (Puverizette5/4, Fritsch GmbH) for 10 h. Stainless steel bowls and balls with a diameter of 10 mm were used. The ball to powder weight ratio was 10:1 for both series of alloys. A certain amount of the reagents mixture was removed periodically from the reactors for SEM and XRD analyses.

The annealing of the powders milled for 10 h was realized in a corundum tube furnace under a protective atmosphere of pure argon in order to study the microstructural evolution of the alloys.

The alloys powders were studied by x-ray diffraction (XRD) using Cu-K_α radiation, scanning electron microscope (SEM, JEOL-5510), differential scanning calorimeter (DSC-Perkin Elmer) and galvanostate "KRIONA-KR515".

The as-milled and annealed materials were used to prepare metal-hydride electrodes by mixing 100 mg alloy with 30 mg Teflonised carbon black (VULKAN 72 with 10 wt% PTFE). The mixture was pressed at 1240 kg cm^{-2}. An electrode with a shape of pellet with a diameter of about 10 mm and thickness of 1 mm was prepared. The electrode was charged and discharged in a three-electrode cell in 30 wt.% water solution of KOH at room temperature. The reference electrode was Hg/HgO and the counter electrode was a nickel net. The charge and discharge current was 100 mA g^{-1} and 50 mA g^{-1}, respectively.

Potentiostatic measurements of fully charged electrodes were carried out at −0.6 V (vs. Hg/HgO) and room temperature (20 °C) in order to determine the hydrogen diffusion coefficients in the TiNi-type alloys.

3 Results and discussion

3.1 Morphology and microstructure of the as-milled alloys

Two series of TiNi ternary alloys for hydrogen storage were synthesized by MA in planetary type mills. In the first series, both Ti and Ni were partially substituted by Zr, V and Cu, Mn, respectively ($Ti_{0.8}M_{0.2}Ni$ (M = Zr, V) and $TiNi_{0.8}N_{0.2}$ (N = Cu, Mn)). In the second series Ni was replaced by Mn in various quantities ($TiNi_{1-x}Mn_x$; $x = 0.2$, 0.4, 0.6, 1.0).

SEM of the as-milled powders revealed particles in the range of 1–15 μm with an average size of about 5 μm and agglomerates of smaller particles (<1–2 μm), Fig. 1. The particles posses a lamellar particle structure as well as a presence of cleavages was observed (Fig. 1). Visible difference in the particles morphology of the different alloys was not detected though the particle size of the $TiNi_{1-x}Mn_x$ series is slightly larger.

X-ray diffraction patterns of the first series as-milled TiNi alloys are presented in Fig. 2. The alloys display a broad diffraction peak around 42–42.5° (2θ) with a shoulder at about 36° and a less intensive one at 60–61° (2θ). In general, the XRD results reveal that the alloying has been successfully realized for all compositions considered, resulting in an extremely fine nanocrystalline material. It has to be mentioned that the diffraction peak at

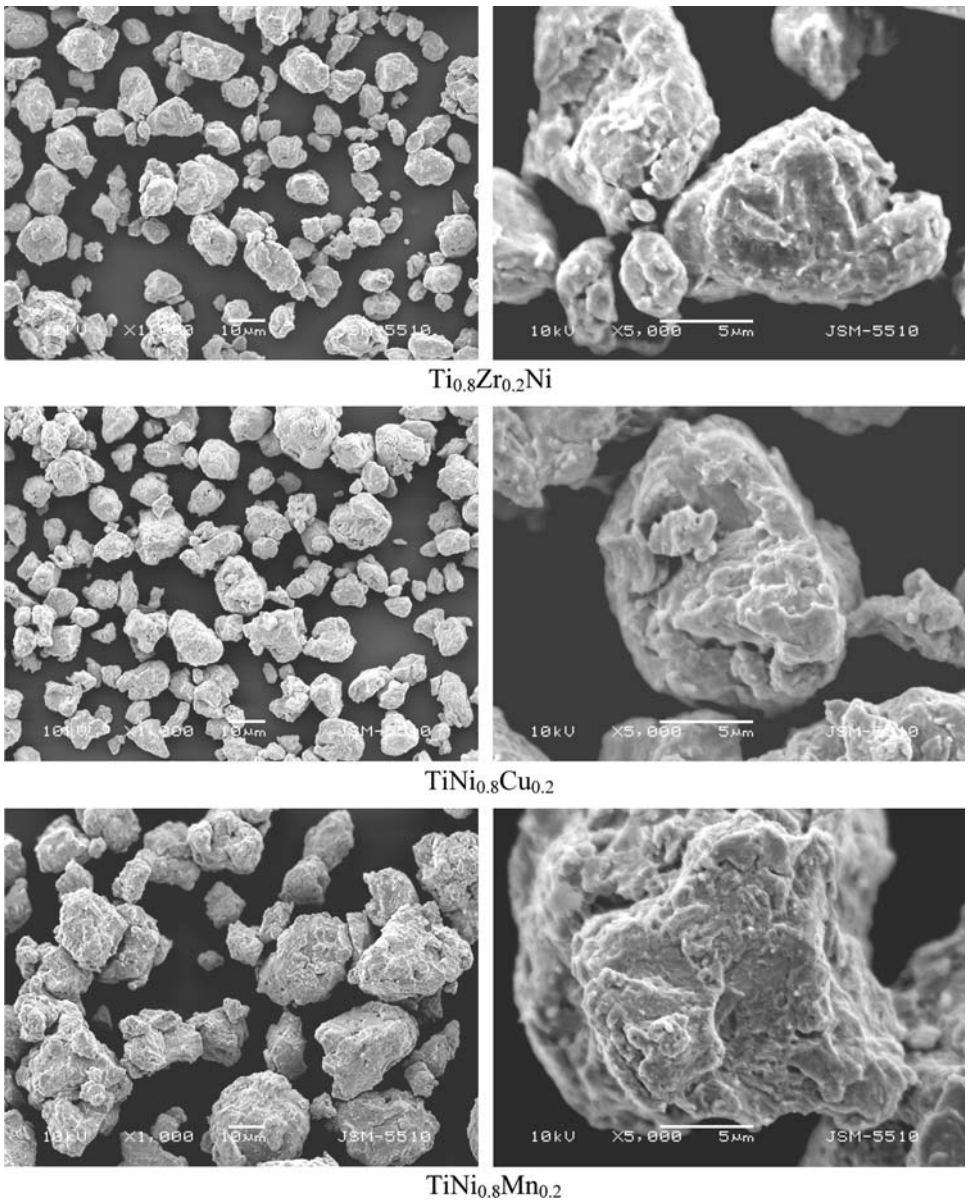

Fig. 1 SEM micrographs of as-milled TiNi alloys

36° is less intensive for the alloy containing V. The position of the very broad diffraction peaks corresponds to the cubic (CsCl type) TiNi phases with slight variations, depending on the alloying element. Compared with recently studied $TiNi_{0.8}M_{0.2}$ (M = Co, Fe, Sn) alloys [14] it can be concluded that among all investigated alloying elements the addition of Sn favors to the largest extent the grain size refinement of TiNi alloys during ball milling.

Figure 3 shows the XRD patterns of the as-milled $TiNi_{1-x}Mn_x$ ($x = 0.2$, 0.4) alloys. This series of alloys contains a larger amount of disordered (amorphous) phase, probably due to the higher energy of the used planetary ball mill, compared to the milling conditions applied for the first series of alloys.

3.2 Electrochemical hydriding/dehydriding of the as-milled alloys

The electrodes prepared from the as-milled alloys were charged for 1 h at current density of 100 mA g^{-1} and discharged at 50 mA g^{-1} to cut-off potential of −650 mV vs. Hg/HgO. A discharge plateau was not observed for any of the compositions. The capacity as a function of the charge/discharge cycle number for the first series is presented in Fig. 4a. The manganese-containing alloy possesses the highest discharge capacity, while the one with copper—the lowest. Fig. 4b shows the same function for the second series of compositions. There is a capacity increase with the cycle number for $TiNi_{0.8}Mn_{0.2}$ and

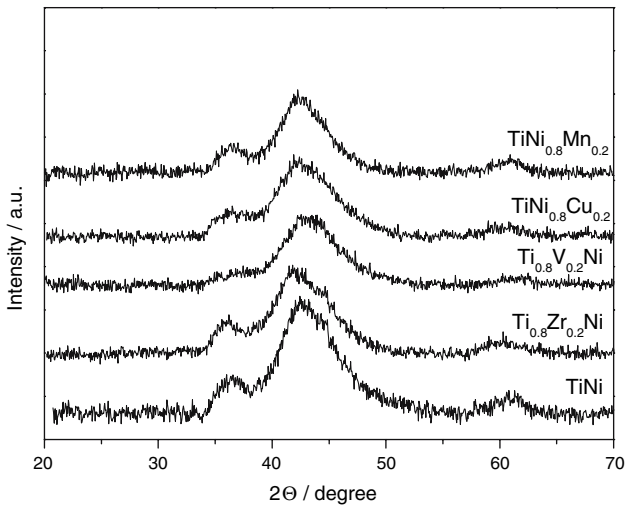

Fig. 2 X-ray diffractograms of the as-milled $Ti_{0.8}M_{0.2}Ni_{0.8}N_{0.2}$ (M = Zr, V; N = Cu, Mn) alloys

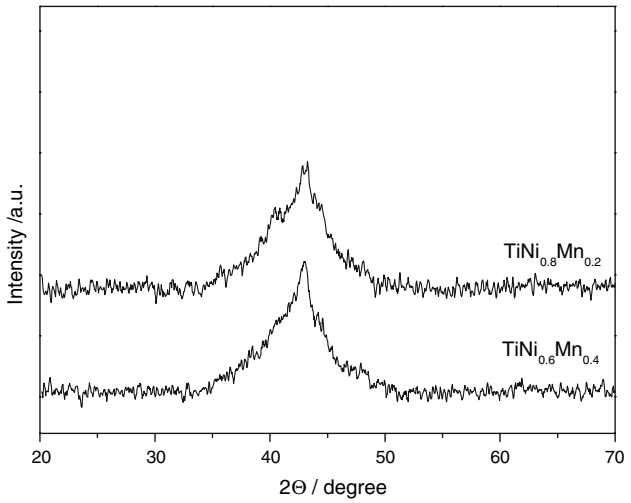

Fig. 3 X-ray diffractograms of the as-milled $TiNi_{1-x}Mn_x$ ($x = 0.2$, 0.4) alloys

$TiNi_{0.6}Mn_{0.4}$ and fast decreasing in the first cycles for $TiNi_{0.4}Mn_{0.6}$ and TiMn. The compositions $TiNi_{0.8}Mn_{0.2}$ and $TiNi_{0.6}Mn_{0.4}$ have almost the same capacity of about 90 mAh g^{-1}, while those with a large amount of Mn displayed higher discharge capacity at the first cycle. It must be underlined that during the discharge process oxidation of manganese to MnO_2 (at different extent) is observed for all studied alloys. The corrosion process is strongest for the TiMn system. This results in higher initial capacity, followed by a fast decreasing at the first several discharges of $TiNi_{0.4}Mn_{0.6}$ and TiMn.

To summarize, the comparison of electrochemical hydriding/dehydriding behavior of the ball milled TiNi-type alloys in the present study, combined with the results of our recent work [14], leads to the conclusion that the replacement of Ni by Mn improves the discharge capacity

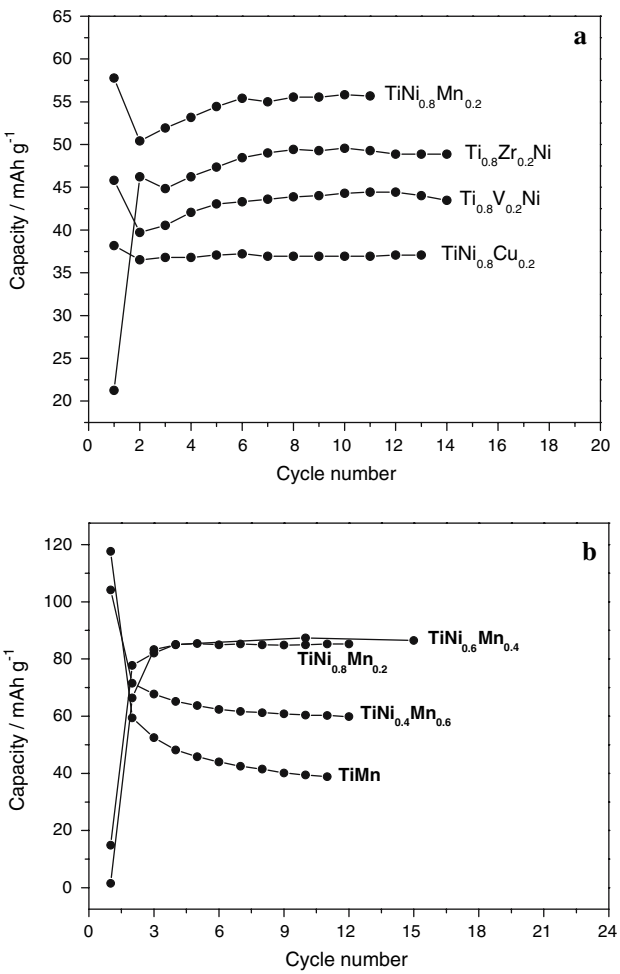

Fig. 4 Capacity as a function of cycle number for the different as-milled compositions

of the alloy in a manner similar to the Fe and Co substitution of Ni in TiNi [14], Fig. 5. An optimum Mn addition in the range of $x = 0.2$–0.4 was determined as well,

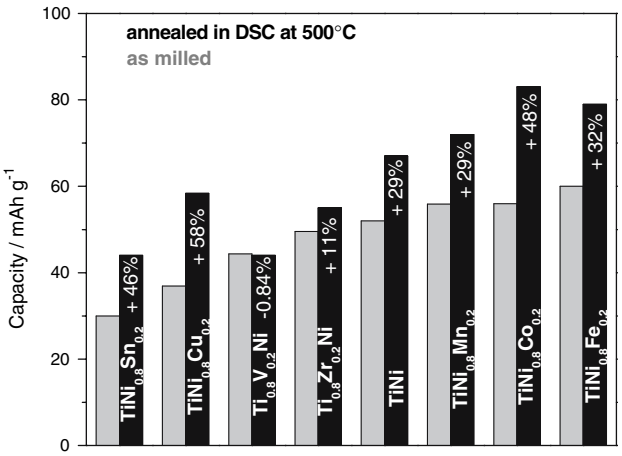

Fig. 5 Capacity for different TiNi alloys before and after annealing

Fig. 4b. Additionally, it was found that finer nanocrystalline/amorphous microstructure results in higher electrochemical capacity of $TiNi_{0.8}Mn_{0.2}$ alloys.

3.3 Thermal stability of the ball-milled alloys

The thermal behavior of the as-milled TiNi alloys, studied by DTA in the temperature range of 50–700 °C, is shown in Fig. 6. An exothermic peak around 500–530 °C is observed for all compositions, as for $TiNi_{0.8}Mn_{0.2}$ this effect is less clearly visible. This thermal effect most probably has to be associated with crystallization of amorphous phase, formed during milling. The as-milled $Ti_{0.8}Zr_{0.2}Ni$ also reveals several broad exothermic peaks in the range 380–480 °C, which can be explained via the occurrence of solid-state reactions between the fine metal powders, unreacted completely during milling. The endothermic effect (450 °C), observed more clearly for $TiNi_{0.8}Cu_{0.2}$, is similar to that of the ball-milled $TiNi_{0.8}(Fe, Co)_{0.2}$ alloys, described in our recent study [14] and deserves additional study. It is, however, interesting to note that the processes associated with the endothermic effects (characterized by a large enthalpy change) do not change the microstructure of the ball milled alloys noticeably, i.e. the materials annealed at 500 °C, which is a temperature just after the endothermic peak (before the exothermic one), are still in a fine nanostructured state, Fig. 7. Neither the position of the broad diffraction peak nor its width changes noticeably after this annealing (500 °C). The average nanocrystals size of the annealed samples (500 °C) varies between 6 and 8 nm for the studied alloys.

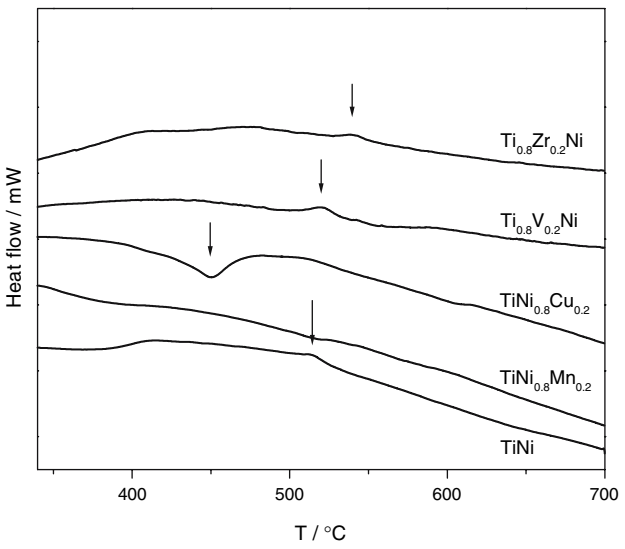

Fig. 6 DTA curves of as-milled TiNi-based alloys (heating rate 10K/min)

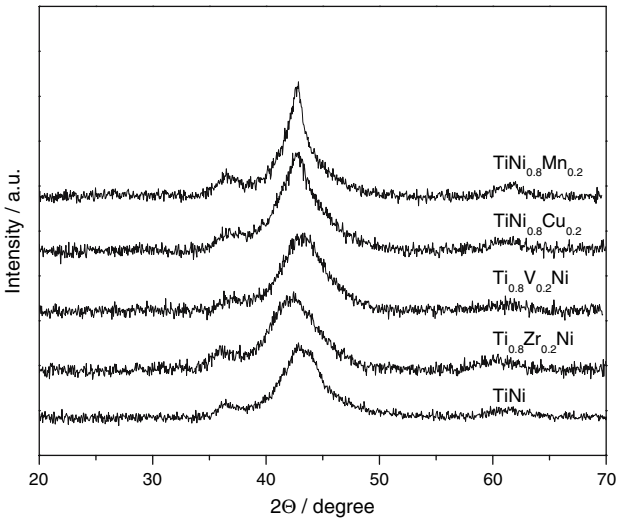

Fig. 7 XRD diffractograms of the annealed $Ti_{0.8}M_{0.2}Ni_{0.8}N_{0.2}$ (M = Zr, V; N = Cu, Mn) alloys

Annealing at two different temperatures (530 °C and 700 °C for 1 h) above the exothermic effect of the as-milled TiNi alloy was applied and the corresponding crystallization and phase transformations were determined by XRD (Fig. 8). This presents the evolution of the microstructure of as-milled TiNi during annealing at different temperatures. Whereas annealing at 500 °C (just before the exothermic effect) leads only to slight narrowing of the broad diffraction peak, immediately after the exothermic peak the diffraction pattern changes distinctly. The most intensive diffraction peaks of the cubic TiNi and Ni_2Ti become sharper, revealing a nanocrystals growth due to the annealing at 530 °C. Further increase in annealing temperature to 700 °C results in additional narrowing of

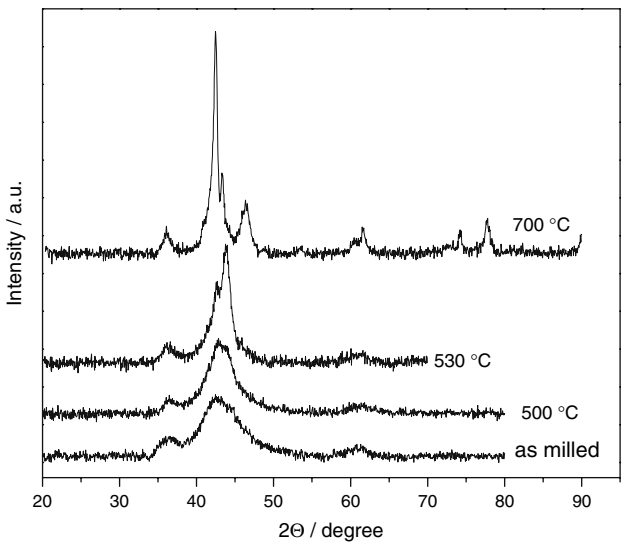

Fig. 8 XRD diffractograms of as-milled and annealed TiNi alloy

the diffraction peaks of the two phases, since the intensity of the cubic TiNi phase increases substantially at the expense of the Ni_2Ti peaks. However, some Ni_2Ti is still present in the annealed alloy after annealing at 700 °C. Obviously, annealing at slightly higher T or for a longer time at 700 °C is necessary to fully transform the ball-milled alloy to the cubic TiNi. For comparison, Szajek et al. [12] indicated that annealing amorphous TiNi for 0.5 h at 700 °C results in complete transformation of the alloy into the cubic TiNi.

3.4 Hydriding properties of the annealed alloys

The hydrogen charge/discharge behavior of the $Ti_{0.8}M_{0.2}$-$Ni_{0.8}N_{0.2}$ (M = Zr, V; N = Cu, Mn) alloys, annealed for short time at 500 °C are different, compared to that in the as milled state. Activation processes and capacity increase with cycling were observed, Fig. 9. $TiNi_{0.8}Mn_{0.2}$ shows the shortest activation (5 cycles) and highest capacity of 75 mAh g^{-1}, comparable to the capacity of the annealed at 500 °C $TiNi_{0.8}Fe_{0.2}$ and $TiNi_{0.8}Co_{0.2}$ alloys [14]. Figure 5 generalizes the maximum capacities of the nanocrystalline TiNi-based ternary alloys in the as-milled state and after annealing at 500 °C from this and a previous study. Except for the vanadium substituted TiNi ($Ti_{0.8}V_{0.2}Ni$) alloy the annealing results in capacity improvement with 10–60%, as the Cu and Co replacement of Ni shows the most beneficial effect of the annealing on the discharge capacity of TiNi. Our results correspond to earlier studies indicating that amorphous and extremely fine nanocrystaline materials reveal lower hydrogen storage capacity than the corresponding well-crystallized nanostructured materials [12, 18]. The main effect of the annealing on the hydriding/dehydriding process is the release of microstresses and grain growth, resulting in an increase of the well-established diffusion paths for the hydrogen atoms along the numerous grain boundaries [12].

Annealing at higher temperatures (e.g. 530 °C), after the exothermic DTA peak, associated with crystallization of the amorphous phase obtained by milling (Fig. 8), does not lead to capacity improvement of TiNi; on the contrary the capacity decreases to values lower than that of the as-milled alloy (<50 mAh g^{-1}).

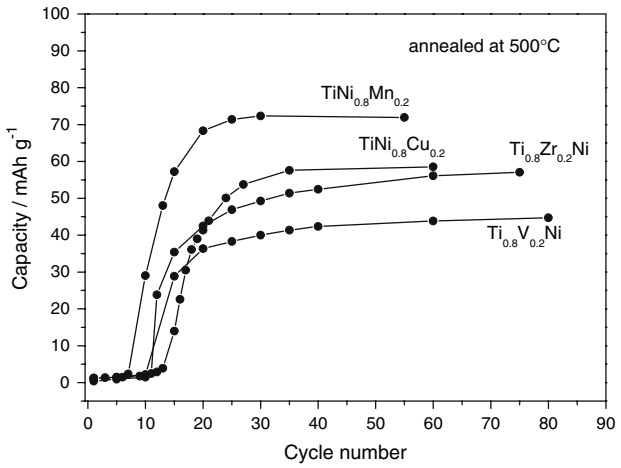

Fig. 9 Capacity as a function of cycle number for annealed TiNi based alloys

3.5 Hydrogen diffusivity in as-milled and annealed TiNi

The hydrogen diffusion coefficients (D_H, cm^2 s^{-1}) in TiNi alloys in different microstructural states were determined by constant potential discharge. A fully charged electrode was discharged at a constant potential of E = −650 mV vs. Hg/HgO. Figure 10 shows discharge curves in

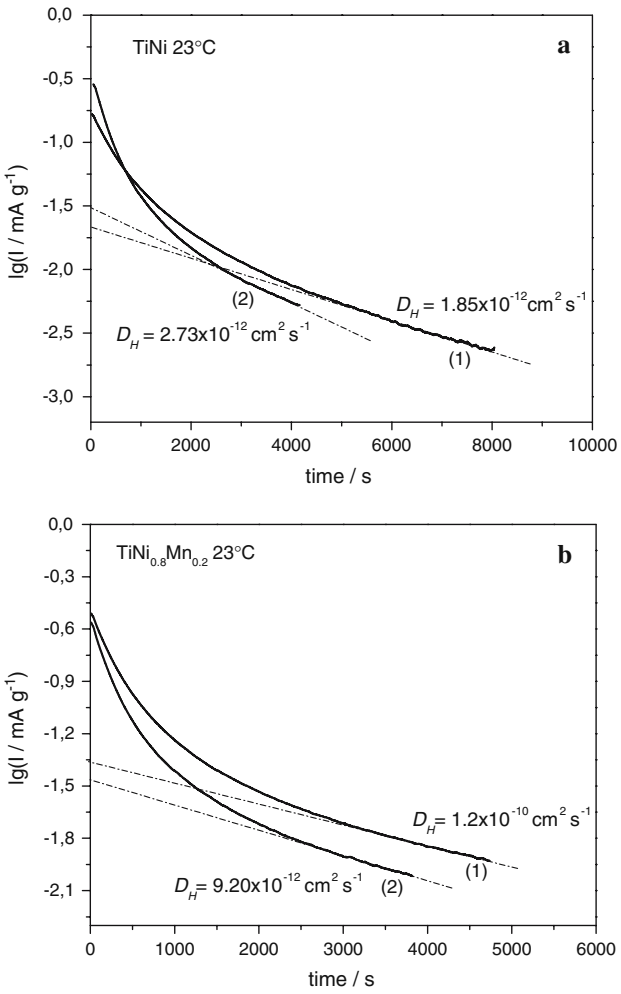

Fig. 10 Potentiostatic discharge of (**a**) fully charged TiNi electrode before (curve 2) and after annealing (curve 1) at 530 °C and (**b**) fully charged $TiNi_{0.8}Mn_{0.2}$ electrode with different microstructure—amorphous state (curve 1), nanostructured (curve 2)

coordinates lg$I$ vs. time (t), where I is a current density expressed in A g^{-1}. In the linear part of the curves hydrogen diffusion within the bulk of the alloy is the rate-determining step, which is characterized by a slow current decrease. From this linear part, it is possible to estimate the average coefficient of diffusion of hydrogen, D_H, in the electrode using the following equation, which is valid at sufficiently large t [19]:

$$\lg I = \left[\frac{6FD_H}{da^2}(C_0 - C_s)\right] - \frac{\pi^2 D_H}{2.303a^2}t$$

where C_0 is the initial hydrogen concentration in the bulk, C_s the hydrogen concentration at the electrode surface, F the Faraday constant, d the density of the material and a the average radius of the particles, which are assumed to have spherical form [20, 21]. According to this equation, the values of D_H were calculated for as-milled and annealed (530 °C) TiNi and for as-milled $TiNi_{0.8}Mn_{0.2}$ with two different microstructures, Table 1. The hydrogen diffusion coefficients of the nanocrystalline TiNi alloys with a small difference in the microstructure are comparable (2.73×10^{-12} and 1.85×10^{-12} cm^2 s^{-1}); that of the as-milled alloy shows a slightly higher value. The diffusion coefficient of hydrogen in the as-milled amorphous/nanocrystalline $TiNi_{0.8}Mn_{0.2}$ was found to be 3–4 times larger than that of the as-milled nanocrystalline alloy with the same composition. For the last two alloys different particle size was determined and, consequently, used for the hydrogen diffusion coefficient calculation. The difference in the particle size results from the different regime of milling applied for the two alloys. Extrapolating the temperature dependence of D_H, reported by Schmidt et al. [17] for NiTi alloy in the temperature range 500–950 °C, a value of 3.2×10^{-11} cm^2 s^{-1} was determined for the diffusion coefficient of hydrogen at room temperature, which is very close to that determined in the present study. Similar D_H-values, determined by electrochemical impedance spectroscopy (EIS), were reported by Mathlouthi et al. [22] for LaNi4Fe (2.7×10^{-10} cm^2 s^{-1}), 1.4×10^{-10} cm^2 s^{-1} for $LaNi_{4.5}Mn_{0.5}$ and 2.7×10^{-10} cm^2 s^{-1} for $LaNi_{3.55}Mn_{0.4}Al_{0.3}Co_{0.75}$. The values, obtained by cyclic voltamometry (CV), were $8.1 \times 10^{8-}$$cm^2$ s^{-1} for $LaNi_4Fe$, $2.5 \times 10^{7-}$ cm^2 s^{-1} for $LaNi_{4.5}Mn_{0.5}$ and $1.5 \times 10^{7-}$ cm^2 s^{-1} for $LaNi_{3.55}Mn_{0.4}Al_{0.3}Co_{0.75}$ [22].

Table 1 Particle size (radius, a) and diffusion coefficient of hydrogen (D_H) in TiNi alloys with different microstructure

Alloy	State	a/μm	D_H/cm^2 s^{-1}
TiNi	As-milled (nano)	2.5	2.73×10^{-12}
TiNi	Annealed, 530 °C (coarser nano)	2.5	1.85×10^{-12}
$TiNi_{0.8}Mn_{0.2}$	As-milled (nano)	2.5	9.20×10^{-12}
$TiNi_{0.8}Mn_{0.2}$	As-milled (amorph/nano)	10	1.20×10^{-10}

4 Conclusion

Nanostructured $Ti_{0.8}M_{0.2}Ni$ (M = Zr, V), $TiNi_{0.8}N_{0.2}$ (N = Cu, Mn) and $TiNi_{1-x}Mn_x$ (x = 0.2, 0.4, 0.6, 1.0) alloys were synthesized by mechanical alloying. $TiNi_{1-x}Mn_x$ (x = 0.2, 0.4, 0.6, 1.0) alloys contain larger amount of amorphous phase than the $Ti_{0.8}M_{0.2}Ni_{0.8}N_{0.2}$ (M = Zr, V; N = Cu, Mn) series due to the higher intensity of milling, which crystallizes during annealing at about 520–530 °C. Whereas annealing of the as-milled nanocrystalline materials at 500 °C results only in slight coarsening of the nanostructure, annealing at 530 °C leads to crystallization of the amorphous phase formed during milling. Fully crystalline material, consisting of mainly cubic TiNi was obtained by annealing at T ≥ 700 °C.

Electrochemical hydrogen charge/discharge measurements of the as-milled, as well as annealed alloys, carried out under galvanostatic conditions, revealed that among the $Ti_{0.8}M_{0.2}Ni$ (M = Zr, V) and $TiNi_{0.8}N_{0.2}$ (N = Cu, Mn) alloys $TiNi_{0.8}Mn_{0.2}$ revealed the highest discharge capacity of 56 mAh g^{-1} in the as-milled state and 75 mAh g^{-1} after annealing at 500 °C. Annealing at higher temperatures does not further increase the capacity. Noticeably higher discharge capacity and better cycle life have been determined for the as-milled $TiNi_{1-x}Mn_x$ alloys with $x \leq 0.4$ compared to the Mn-richer alloys.

The hydrogen diffusion coefficients into TiNi alloys with fine nanocrystalline microstructure (as-milled) and with coarser nanostructure (annealed at 500 °C) as well as of as-milled $TiNi_{0.8}Mn_{0.2}$ with two different microstructures were determined. The hydrogen diffusion coefficients of the TiNi alloys are comparable, as this of the as-milled alloy shows slightly higher value (2.73×10^{-12} cm^2 s^{-1}). The diffusion coefficient of hydrogen in the amorphous $TiNi_{0.8}Mn_{0.2}$ was found to be higher than that of the nanocrystalline alloy with the same composition.

Acknowledgments The work was supported by the Bulgarian Scientific Research Fund under grant BYX-14/05 and by the National Science Fund, Project "University research center on nanotechnologies and new materials".

References

1. Reilly JJ, Wiswall RH (1974) J Inorg Chem 13:218
2. Buschow KHJ, Bouten PCP, Miedema AR (1982) Rep Prog Phys 45:937
3. Sandrock GD, Goodell PD (1980) J Less-Common Met 73:161
4. Luan B, Cui N, Liu HK, Zhao HJ, Dou SX (1985) J Power Sources 55:236

5. Lee SM, Perng TP (1999) J Alloys Compd 291:254
6. Jurczyk M, Jankowska E, Nowak M, Jakubowicz J (2002) J Alloys Compd 336:265
7. Jankowska E, Jurczyk M (2002) J Alloys Compd 346:L1–L3
8. Ruggeri S, Roue L, Huot J, Schultz R, Aymard L, Tarascon JM (2002) J Power Sources 112:547
9. Jakubowicz J (2004) J Mat Sci 39:5379
10. Jankowska E, Jurczyk M (2004) J Alloys Compd 372:L9–L12
11. Jurczyk M (2004) Bull Pol Ac: Tech 52:67
12. Szajek A, Makowiechka M, Jankowska E, Jurczyk M (2005) J Alloys Compd 403:323
13. Wang CS, Lei YQ, Wang QD (1998) J Power Sources 70:222
14. Drenchev B, Spassov T (2007) J Alloys Compd 441:197–201
15. Sandrock G (1999) J Alloys Compd 293–295:877–888
16. Lee S-M, Perng T-P (1999) J Alloys Compd 291:254–261
17. Schmidt R, Schlereth M, Wipf H, Assmus W, Muellner M (1989) J Phys Condens Matter 1:2473–2482
18. Zaluski L, Zaluska A, Ström-Olsen JO (1997) J Alloys Compd 253–254:70
19. Zheng G, Popov BN, White RE (1995) J Electrochem Soc 8:2695
20. Nishina T, Ura H, Uchida I (1996) J Electrochem Soc 143:1287
21. Ura H, Nishina T, Uchida I (1995) J Electroanal Chem 142:2695
22. Mathlouthi H, Khaldi C, Ben Moussa M, Lamloumi J, Percheron-Guégan A (2004) J Alloys Compd 375:297